Parallel Implementation of the Four-Component Relativistic Quasidegenerate Perturbation Theory with General Multiconfigurational Reference Functions

Ryo Ebisuzaki,[†] Yoshihiro Watanabe,[†] Yukio Kawashima,[†,‡] and Haruyuki Nakano*[,†]

[†]Department of Chemistry, Graduate School of Sciences, Kyushu University, Fukuoka 812-8581, Japan
[‡]Institute of Advanced Research, Kyushu University, Fukuoka 812-8581, Japan

ABSTRACT: A new, efficient parallel algorithm for four-component relativistic generalized multiconfigurational quasidegenerate perturbation theory (GMC-QDPT) introducing Kramers symmetry is implemented. Because it utilizes the independence of the terms in the matrix element computations, this algorithm both speeds up the calculation and reduces the computational resources required for each node. In addition, the amount of memory for two-electron integrals is reduced to three-eigths by Kramers restriction. The algorithm is applied to the d−d excitation energies of the platinum halide complexes, $[PtCl_4]^{2-}$, $[PtBr_4]^{2-}$, and $[PtCl_6]^{2-}$ and to the 6p−7s and 6p−7p excitation energies of the radon atom. It is shown to provide high parallelization efficiency and accurate excitation energies that agree well with experimental data.

1. INTRODUCTION

In electronic structure calculations for systems that contain heavy elements, the inclusion of both the electron correlation and relativistic effects is essential for high accuracy. Thus, many electron correlation methods have been extended to four-component relativistic versions, including Møller−Plesset perturbation,[1−5] configuration interaction (CI),[6,7] and coupled cluster methods,[8,9] which are based on the Dirac−Hartree−Fock (DHF) reference wave function. In addition, four-component multireference (MR) CI[10−12] and coupled cluster[13] methods that provide highly accurate molecular electronic structures are also now available. However, the four-component MR methods are computationally expensive, and their applications are therefore limited to small molecules.

Among the MR methods, multireference perturbation theory (MRPT) is efficient and accurate and thus is regarded as a practical tool that takes account of both static and dynamic electron correlations. Recently, we developed a MRPT using the general multiconfigurational functions called GMC-QDPT or GMC-PT.[14] GMC-QDPT is applicable to any multiconfigurational reference wave functions and allows the use of only necessary configurations according to the character of the system of interest. Because of its generality and flexibility, GMC-QDPT enjoys both high computational accuracy and efficiency. However, it is still not easy to calculate heavy atom compounds with many electrons efficiently using relativistic GMC-QDPT.[15] Therefore, there is a need for computational schemes for relativistic GMC-QDPT that are more efficient than the existing one.

Previously, we proposed a new efficient calculation scheme for the effective Hamiltonian based on matrix elements between the reference and ionized functions and succeeded in reducing computation time relative to the previous scheme.[16] In the present work, we developed a parallel algorithm based on Kramers symmetry. For the nonrelativistic MC-QDPT, Umeda and co-workers have presented a parallel algorithm.[17] This algorithm was based on the previous scheme of ours using diagrams and thus has a disadvantage for the computation of one virtual terms (the terms involving two-electron integrals with one virtual and three occupied orbital labels) of the effective Hamiltonian.[16] In addition, we applied the new code accelerated by our parallel algorithm to the calculations for the d−d excitation energies of platinum halide complexes ($[PtCl_4]^{2-}$, $[PtBr_4]^{2-}$, and $[PtCl_6]^{2-}$) and the 6p−7s/6p−7p excitation energies of the radon atom.

In Section 2, we review GMC-QDPT and describe our new parallel algorithm and its implementation. We report the efficiency of our new scheme and the accuracy of the excitation energy calculation results in Section 3.

2. METHODS

2.1. Brief Review of GMC-QDPT. Before describing the new computational scheme, we briefly review the GMC-QDPT for readers' convenience.

Let $|\mu\rangle$ and $E_\mu^{(0)}$ be reference (zeroth-order) wave functions and their zeroth-order energies:

$$|\mu\rangle = \sum_{A \in \text{GCS}} C_A^\mu |A\rangle, \qquad E_\mu^{(0)} = \sum_p \langle\mu|a_P^\dagger a_P|\mu\rangle \varepsilon_P \quad (1)$$

respectively. Here, the reference wave functions $|\mu\rangle$ are expanded by the determinants $|A\rangle$ in a general configuration space (GCS); $a_P^\dagger$ and a_P are the creation and annihilation

operators, respectively, for an electron in spinor P; and ε_P are spinor energies. The effective Hamiltonian up to the second order of GMC-QDPT[14,15] is given as

$$(H_{\text{eff}}^{(0-2)})_{\mu\nu} = \langle\mu|H|\nu\rangle$$

$$-\frac{1}{2}\left\{\sum_{I \notin \text{GCS}} \frac{\langle\mu|H|I\rangle\langle I|H|\nu\rangle}{E_\nu^{(0)} - E_I^{(0)}} + \sum_{I \notin \text{GCS}} \frac{\langle\mu|H|I\rangle\langle I|H|\nu\rangle}{E_\mu^{(0)} - E_I^{(0)}}\right\} \tag{2}$$

where $|I\rangle$ is the determinant outside the GCS.

We define the corresponding complete active space (CCAS) as the minimal CAS including the reference GCS. The summation over $|I\rangle$ can be divided into a summation outside the CCAS and a summation inside the CCAS but outside the GCS. Thus, the summation enclosed in curly brackets in eq 2 can be written as

$$(H_{\text{eff}}^{(2)})_{\mu\nu}$$

$$= \sum_{I \notin \text{CCAS}} \frac{\langle\mu|H|I\rangle\langle I|H|\nu\rangle}{E_\nu^{(0)} - E_I^{(0)}} + \sum_{I \in \text{CCAS} \wedge I \notin \text{GCS}} \frac{\langle\mu|H|I\rangle\langle I|H|\nu\rangle}{E_\nu^{(0)} - E_I^{(0)}} \tag{3}$$

We call the terms in the first summation "the external terms" and the terms in the second summation "the internal terms".[14]

The internal terms are computed through matrix operations for the Hamiltonian matrix. The length of the internal term summation is generally much less than that of the external term summation. Hence, the computational time for the internal terms is small compared with that for the external terms.

The external terms are computed using a matrix element scheme.[16] The intermediate states $|I\rangle$ can be written as a product of determinants comprising M active spinors $|B^M\rangle$ and ionization/excitation operators:

$$E_{QS\ldots U}^{PR\ldots T} = a_P^\dagger a_R^\dagger \ldots a_T^\dagger a_U \ldots a_S a_Q \tag{4}$$

(abbreviated as E_X). Note that the numbers of creation and annihilation operators are not necessarily equal.

Hence, the summation of the external terms is expressed as

$$(H_{\text{external}}^{(2)})_{\mu\nu} = \sum_X \sum_{B^M} \frac{\langle\mu|HE_X|B^M\rangle\langle B^M|E_X^\dagger H|\nu\rangle}{E_\nu^{(0)} - E_{XB^M}^{(0)}} \tag{5}$$

where $E_{XB^M}^{(0)}$ are zeroth-order energies of $E_X|B^M\rangle$. In this scheme, we calculate eq 5 as the summation of the product of each matrix element $\langle\mu|HE_X|B^M\rangle$. There are five combinations of E_X and $|B^M\rangle$ that give nonzero $\langle\mu|HE_X|B^M\rangle$. Each matrix element can be simplified through normal ordering of creation and annihilation operators. These can be divided into two categories based on the number of virtual spinor labels. We define the terms with one or no virtual spinor label as 1-virtual terms and other terms with two virtual spinor labels as 2-virtual terms. For example, one of the 1-virtual

terms is

$$\langle\mu|HE^E|B^{N-1}\rangle = \sum_P f_{PE}^{\text{core}}\langle\mu|E^P|B^{N-1}\rangle$$

$$+ \frac{1}{2}\sum_{PRS}(PE\|RS)\langle\mu|E_S^{PR}|B^{N-1}\rangle$$

$$= \sum_P \sum_A f_{PE}^{\text{core}} C_A^{\mu*}\langle A|E^P|B^{N-1}\rangle$$

$$+ \frac{1}{2}\sum_{PRS}\sum_A(PE\|RS)C_A^{\mu*}\langle A|E_S^{PR}|B^{N-1}\rangle \tag{6}$$

and one of the 2-virtual terms is

$$\langle\mu|HE^{EF}|B^{N-2}\rangle = \frac{1}{2}\sum_{PR}(PE\|RF)\langle\mu|E^{PR}|B^{N-2}\rangle$$

$$= \frac{1}{2}\sum_{PR}\sum_A(PE\|RF)C_A^{\mu*}\langle A|E^{PR}|B^{N-2}\rangle \tag{7}$$

where E and F are virtual spinor labels; I and J are core spinor labels; P, Q, and R are active spinor labels; N is the number of active electrons; f_{PE}^{core} are the core Fock matrix elements; $(PQ\|RS)$ are the antisymmetrized two-electron integrals; and $\langle A|E_X|B^M\rangle$ are the coupling coefficients (CCs).

2.2. Parallel Algorithm. A feature of the perturbation method at the second order is that the energy or effective Hamiltonian is expressed as a summation of many independent terms. Neither diagonalization of large matrices nor solution of large linear equations is necessary. Specifically, the terms for determinant B^M and ionization operator X in eq 5 are independent of each other. In addition, the matrix elements used to obtain the terms in eq 5 are also simple sums of the product of molecular integrals, CI coefficients, and CCs, as seen in eqs 6 and 7.

The most straightforward method of parallelization is to use the independency of the terms for the determinants B^M in eq 5. The summation for B^M can be computed easily in parallel after being divided and assigned to computational nodes. In fact, the speedup by parallel computing was almost linear with the number of computational nodes in our preliminary calculations. However, in this parallelization, all molecular integrals are required for each node, and thus no scalability is gained for integral storage, which is a real problem in practice. Therefore, parallelization was done utilizing the independency of the terms in the matrix element computations of eqs 5 and 6.

In the serial algorithm, the Hamiltonian matrix elements and their associated effective Hamiltonian matrix elements are calculated according to Schemes 1 and 2 for $\langle\mu|HE^E|B^{N-1}\rangle$ and $\langle\mu|HE^{EF}|B^{N-2}\rangle$, respectively. The algorithm is coupling coefficient driven. For each ionized determinant $|B^M\rangle$, all nonzero coupling coefficients $\langle A|E_X|B^M\rangle$ ($= +1$ or -1) are calculated first. Then, being operated by an ionization operator E_X, intermediate determinants $|I\rangle = E_X|B^M\rangle$ are made, and the matrix elements $\langle\mu|HE_X|B^M\rangle$ are computed. Finally, the effective Hamiltonian elements are computed.

The steps specific on the parallel algorithm are emphasized in bold in Schemes 1 and 2. Consider Scheme 2 as an example to explain the parallel algorithm. Usually, the computational cost of the coupling coefficients $\langle A|E_X|B^M\rangle$ is much smaller than that of the matrix elements $\langle\mu|HE_X|B^M\rangle$. For each B^{N-2}, the operation count for $\langle A|HE^{PR}|B^{N-2}\rangle$ is $O(m_{\text{act}}^2)$, where m_{act} is the number of active spinors, while the operation count for $\langle\mu|HE^{EF}|B^{N-2}\rangle$ is $O(m_{\text{act}}^2 m_{\text{vir}}^2)$, where m_{vir} is the number of virtual spinors. Thus, in

Scheme 1. Loop Structure for the Effective Hamiltonian Contributed From 1-Virtual Integrals[a]

```
Loop over ionized determinants |B^{N-1}⟩
   a. Calculate all nonzero coupling coefficients (CCs) ⟨A|E^P|B^{N-1}⟩
      for |B^{N-1}⟩
   b. Calculate all nonzero CCs ⟨A|E_S^{PR}|B^{N-1}⟩ (P<R) for |B^{N-1}⟩
   c. Distribute E to computational nodes
   d. On each node: Loop over E assigned to the node
      (1) Clear h(...)
      (2) Loop over nonzero CCs ⟨A|E^P|B^{N-1}⟩
        Loop over reference states μ
           If ⟨A|E^P|B^{N-1}⟩=±1, h(μ)=h(μ)±f_{PE}^{core}C_A^{μ*}
      (3) Loop over nonzero CCs ⟨A|E_S^{PR}|B^{N-1}⟩
        Loop over reference states μ
           If ⟨A|E_S^{PR}|B^{N-1}⟩=±1, h(μ)=h(μ)±(PE∥RS)C_A^{μ*}
      (4) Loop over reference states μ and ν
        H_eff(μ,ν)=H_eff(μ,ν)+h(μ)·h(ν)^*/(E_ν^{(0)}-E_{B^{N-1}}^{(0)}-ε_E)
   e. Calculate global sum of H_eff(...,...)
```

[a] The steps required in parallel algorithm are shown in bold.

Scheme 2. Loop Structure for the Effective Hamiltonian Contributed From 2-Virtual Integrals[a]

```
Loop over ionized determinants |B^{N-2}⟩
   a. Calculate all nonzero coupling coefficients (CCs) ⟨A|E^{PR}|B^{N-2}⟩
      (P<R) for |B^{N-2}⟩
   b. Distribute E, F pairs to computational nodes (E<F)
   c. On each node: Loop over E and F assigned to the node
      (1) Clear h(...)
      (2) Loop over nonzero CCs ⟨A|E^{PR}|B^{N-2}⟩
        Loop over reference states μ
           If ⟨A|E^{PR}|B^{N-2}⟩=±1, h(μ)=h(μ)±(PE∥RF)C_A^{μ*}
      (3) Loop over reference states μ and ν
        H_eff(μ,ν)=H_eff(μ,ν)+h(μ)·h(ν)^*/(E_ν^{(0)}-E_{B^{N-2}}^{(0)}-ε_E-ε_F)
   d. Calculate global sum of H_eff(...,...)
```

[a] The steps required in parallel algorithm are shown in bold.

the parallel algorithm, the coupling coefficients are computed first in each computational node. Next, the E, F pairs are divided and assigned to computational nodes. (In other words, the ionization/excitation operators $E_X = E^{EF}$ are distributed.) Then, part of the effective Hamiltonian is calculated on each node for the assigned E, F pairs. Finally, the effective Hamiltonians on respective nodes are collected and summed to obtain the total effective Hamiltonian. The parallel algorithms for the other terms are similar to Schemes 1 and 2.

The speedup by the parallel algorithm is roughly estimated as

$$S_{estimated}(n) = \frac{T_{EH} + T_{CC}}{T_{EH}/n + T_{CC}} \qquad (8)$$

where n is the number of computational nodes, and T_{EH} and T_{CC} are the computational times of the serial algorithm for the perturbation summation and CCs, respectively. As long as T_{CC} is negligible compared with T_{EH}/n (namely $T_{EH}/n \gg T_{CC}$), parallelization is expected to speed up the calculation by a factor of n.

The integral storage is also reduced by a factor n by parallelization. For the 1-virtual terms in Scheme 1, label E and associated integrals $(PE\|RS)$ is distributed to each computational node. Hence the integral storage on a node is reduced to $([(m_{vir} - 1)/n] + 1)m_{vir}^{-1}$ of the total, where the Gauss bracket $[X]$ denotes the largest integer less than or equal to X. For the 2-virtual terms in Scheme 2, since the pair of labels (E,F) and associated integrals $(PE\|RF)$ $(E < F)$ is distributed, the integral storage on a node is reduced to $([\{m_{vir}(m_{vir} - 1)/2 - 1\}/n] + 1)(m_{vir}(m_{vir} - 1)/2)^{-1}$ of the total. These values approach $1/n$ if m_{vir} is sufficiently large compared with n.

2.3. Kramers Restriction (Kramers-Restricted GMC-QDPT Formulas). The original GMC-QDPT was expressed in the

Kramers-unrestricted form as in eqs 6 and 7 to allow for the external magnetic field when needed. However, Kramers-restricted formulas allow us to use only unique integrals in the absence of an external magnetic field, such as the implementation of Yanai et. al[18] in a 4-spinor molecular Dirac—Fock SCF method. In our implementation, we employ Kramers restriction to save memory resources for GMC-QDPT calculation.

The time-reversed function $\bar{\phi} = \phi(-t)$ is written through the time reversal operator $\hat{K}$; as

$$\hat{K}\phi = \bar{\phi}, \qquad \hat{K}\bar{\phi} = -\phi \qquad (9)$$

Using the relation

$$\hat{K}(pq||rs) = (-1)^N (\hat{K}p\hat{K}q||\hat{K}r\hat{K}s)^* \qquad (10)$$

where $\hat{K}p$ is a short expression for $\hat{K}\phi_p$, and N is the number of barred spinors in $\{\phi_p, \phi_q, \phi_r, \phi_s\}$ and the label symmetry:

$$(pq \parallel rs) = -(rq \parallel ps) = -(ps \parallel rq) = (rs \parallel pq) \quad (11)$$

we can reduce the 16 $(= 2^4)$ kinds of 1- and 2-virtual integrals to 6:

$$(pe||rs) = (\overline{pe}||\overline{rs})^*, \qquad (\overline{pe}||\overline{rs}) = -(p\overline{e}||rs)^*$$

$$(pe||r\overline{s}) = -(\overline{pe}||\overline{rs})^*, \qquad (\overline{pe}||\overline{rs}) = (p\overline{e}||r\overline{s})^*$$

$$(pe||\overline{rs}) = -(\overline{pe}||r\overline{s})^* = -(\overline{re}||ps) = (r\overline{e}||\overline{ps})^*$$

$$(\overline{pe}||r\overline{s}) = (p\overline{e}||\overline{rs})^* = -(re||\overline{ps}) = -(\overline{re}||ps)^* \qquad (12)$$

for 1-virtual integrals, and

$$(pe||rf) = (\overline{pe}||\overline{rf})^*, \qquad (\overline{pe}||\overline{rf}) = -(p\overline{e}||rf)^*$$

$$(pe||r\overline{f}) = -(\overline{pe}||\overline{rf})^*, \qquad (\overline{pe}||\overline{rf}) = (p\overline{e}||r\overline{f})^*$$

$$(\overline{pe}||rf) = -(p\overline{e}||\overline{rf})^* = -(re||\overline{pf}) = (\overline{re}||p\overline{f})^*$$

$$(pe||\overline{rf}) = (\overline{pe}||rf)^* = -(\overline{re}||p\overline{f}) = -(r\overline{e}||\overline{pf})^* \qquad (13)$$

for 2-virtual integrals.

By reducing the integrals, we can obtain Kramers-restricted formulas for the matrix elements as eqs 6 and 7. For example, $\langle u|HE^{EF}|B^{N-2}\rangle$ are rewritten as

$$\langle u|HE^{ef}|B^{N-2}\rangle = \frac{1}{2}\sum_{pr}\sum_A \{(pe||rf)C_A^{u*}\langle A|E^{pr}|B^{N-2}\rangle$$

$$+ 2(\overline{pe}||rf)C_A^{u*}\langle A|E^{\overline{pr}}|B^{N-2}\rangle + (\overline{pe}||\overline{rf})C_A^{u*}\langle A|E^{\overline{pr}}|B^{N-2}\rangle\}$$

$$(14)$$

$$\langle u|HE^{\overline{ef}}|B^{N-2}\rangle = \frac{1}{2}\sum_{pr}\sum_A \{(pe||rf)^*C_A^{u*}\langle A|E^{\overline{pr}}|B^{N-2}\rangle$$

$$+ 2(\overline{pe}|rf)^*C_A^{u*}\langle A|E^{p\overline{r}}|B^{N-2}\rangle + (\overline{pe}||\overline{rf})^*C_A^{u*}\langle A|E^{pr}|B^{N-2}\rangle\}$$

$$(15)$$

$$\langle u|HE^{e\overline{f}}|B^{N-2}\rangle = \frac{1}{2}\sum_{pr}\sum_A \{(\overline{pe}||\overline{rf})C_A^{u*}\langle A|E^{p\overline{r}}|B^{N-2}\rangle$$

$$+ 2(pe||r\overline{f})C_A^{u*}\langle A|E^{p\overline{r}}|B^{N-2}\rangle + (pe||r\overline{f})C_A^{u*}\langle A|E^{pr}|B^{N-2}\rangle\}$$

$$(16)$$

(Type $\langle u|HE^{\overline{ef}}|B^{N-2}\rangle$ do not appear because of the restriction $E < F$.) These formulas are actually used in the program.

In contrast to Kramers-unrestricted formulas, the length of the summation for Kramers-pair labels p and r in eqs 14—16 is one-fourth of that for spinor labels P and R in eq 7, whereas the number of terms in the summation has increased from one to three. Therefore, the operation count is hardly reduced. On the other hand, however, we can reduce the amount of memory used to store integrals to about three-eighths $(= 6/16)$.

3. RESULTS AND DISCUSSION

We applied the present computational scheme to some molecular systems and measured CPU time (on 3.0 GHz Pentium D 930 processors) to evaluate its performance. We calculated the d—d excitation energies for three platinum halide anions (d^8-complex $[PtCl_4]^{2-}$, $[PtBr_4]^{2-}$, and d^6-complex $[PtCl_6]^{2-}$), and the 6p—7s and 6p—7p excitation energies of the Rn atom.

The spinors used in the perturbation calculations were determined using the four-component DHF method[19] using the REL4D program[20] of UTChem.[21] The basis set proposed by Koga, Tatewaki, and Matsuoka (KTM)[22] was employed for the platinum halide complex calculations. For Cl, a d basis spinor (exponent 0.514) was added as a polarization function. For Rn, Dyall's triple-ζ[23] basis set, which includes up to g-type polarization function, augmented by single s, p, and d diffuse functions in an even-tempered manner was employed. The molecular structures for the platinum halide complexes were taken from experimental data.[24,25] The zeroth-order wave functions were set according to the scheme for nonrelativistic multireference multi state perturbation theory implemented in Firefly.[26]

3.1. d—d Excitation Energies of Platinum Tetrachloride Dianion $[PtCl_4]^{2-}$. First, we calculated the d—d excitation energies of $[PtCl_4]^{2-}$. The target states were the 12 lowest excited states resulting from d—d single excitations as well as the ground state. The reference CI space was of a multireference singles (MRS) type constructed from 20 electrons and 26 spinors, which include 5d components of the platinum atom largely and therefore necessary to describe the considered excitation states. The determinants that spanned the reference CI space were generated from 41 parent configurations (the DHF configuration and the singly excited configurations constructed from the highest 20 occupied and the lowest 2 unoccupied spinors) and selected according to their weights in the reference functions. The determinants whose weights in the reference wave functions were greater than 10^{-8} (i.e., $|C_I| > 10^{-4}$) were selected. The lowest 108 spinors were frozen in the perturbation calculations. Compared with previous papers,[16] we used larger basis sets that were specifically designed for four-component relativistic calculations.

First, let us discuss the accuracy of the GMC-QDPT results.

The computed excitation energies are summarized in Table 1, together with experimental data from Patterson[27] and the two-component time-dependent density functional theory (TDDFT) results of Wang and Ziegler[28] for comparison. For the states for which experimental data are available (the $2A_{1g}$, $1B_{1g}$—$2B_{1g}$

Table 1. d−d Excitation Energies of $[PtCl_4]^{2-}$ (eV)

state	ref-CI	GMC-QDPT	ref (%)[a]	TDDFT	band	expt
$1A_{1g}$	2.13	1.98	74.3	2.30		
$1A_{2g}$	2.20	2.06	74.4	2.34		
$1E_g$	2.24	2.11	73.6	2.38	1	2.12
$1B_{2g}$	2.31	2.40	67.7	2.49	2	2.24
$1B_{1g}$	2.59	2.47	69.8	2.59	3	2.57
$2E_g$	2.63	2.56	70.8	2.69	3	2.57
$2A_{1g}$	3.15	2.72	73.7	2.98	4	2.97
$3E_g$	3.19	2.94	70.1	3.03	4	2.97
$2A_{2g}$	3.54	3.10	73.9	3.19		
$2B_{2g}$	3.49	3.38	71.5	3.43	5	3.23
$4E_g$	3.85	3.54	73.5	3.50	6	3.67
$2B_{1g}$	3.89	3.82	71.0	3.53	6	3.67

[a] The reference weight of the ground state was 75.5%.

$1B_{2g}−2B_{2g}$, and $1E_g−4E_g$ states), the computed values showed good agreement with experimental values. The maximum and average deviations from the experiment were 0.16 and 0.08 eV, respectively.

Table 1 includes the approximate weight that the reference function occupied in the first-order perturbed wave function.[15] GMC-QDPT enables us to include only configurations necessary to construct the reference wave function, which greatly reduces the computational time and resources needed compared with complete active space self-consistent field (CASSCF) reference perturbation theories. However, we must carefully investigate whether we have considered enough configurations in our calculations, because we reduced a large number of configurations to construct our reference wave function. To investigate our selection of the configurations, the weight of the reference function in the first-order perturbed wave function was examined. This weight is a measure of the quality of the reference wave functions; if the weight is large enough, then we have included enough configurations. By comparing the relative weight calculated for different states, we can investigate the balance of the calculation; if the weights for each state have similar values, then we have included enough configurations to describe all states with the same quality. The weights in Table 1 are close to each other. The values are in the range 67.7−74.4% for the excited states and 75.5% for the ground state, which indicates that the calculations were well balanced.

In comparison with the TDDFT results, the GMC-QDPT excitation energies were smaller, especially in the lowest few excited states. TDDFT calculation results showed a tendency to overestimate the excitation energies, whereas GMC-QDPT results agreed well with the experimental data for this system.

Now, let us discuss the efficiency of the parallel algorithm.

Table 2 summarizes the wall computational time and speedup of the present scheme for the $[PtCl_4]^{2-}$ calculations, and Figure 1 is a plot of speedup ratios. Speedup is defined as $S(n) = T_{seq}/T(n)$, where T_{seq} is the wall clock time of a sequential execution, and $T(n)$ is the wall clock time of a parallel execution on n nodes.

As seen from Figure 1, the total speedup was approximately proportional to the number of nodes n. The speedup values of calculations for internal, 1-virtual, and 2-virtual terms showed different behaviors. Speedup of the calculation for 2-virtual terms was nearly proportional to the number of nodes; by contrast, the calculation for internal terms showed almost no speedup for an

Table 2. Wall Times and Parallel Efficiency of the $[PtCl_4]^{2-}$ Calculations[a]

no. of nodes	wall time (s)					parallel efficiency
	internal part	1-virtual part	2-virtual part	total	speedup	
1	6.51	137.01	1324.93	1468.44	1.00	1.00
2	5.87	72.34	651.59	729.80	2.01	1.01
3	5.68	48.98	428.97	483.64	3.04	1.01
4	5.62	38.94	313.34	357.89	4.10	1.03
5	5.57	33.63	251.18	290.39	5.06	1.01
6	5.55	29.45	206.05	241.06	6.09	1.02
7	5.53	25.78	173.15	204.46	7.18	1.03
8	5.49	24.08	153.23	182.80	8.03	1.00
9	5.44	22.58	134.63	162.65	9.03	1.00
10	5.42	21.31	119.35	146.08	10.05	1.01
11	5.34	20.18	109.40	134.92	10.88	0.99
12	5.34	19.20	98.17	122.72	11.97	1.00
13	5.29	19.05	89.93	114.27	12.85	0.99
14	5.28	17.55	83.66	106.50	13.79	0.98
15	5.29	17.46	77.50	100.25	14.65	0.98
16	5.28	16.75	70.78	92.81	15.82	0.99
20	5.26	15.67	57.96	78.89	18.61	0.93
24	5.22	14.93	48.63	68.78	21.35	0.89
28	5.25	13.23	41.66	60.14	24.42	0.87
32	5.22	13.21	37.25	55.68	26.37	0.82

[a] The wall times for the CC calculations were 5.08, 7.65, and 0.31 s for the internal, 1-virtual, and 2-virtual parts, respectively.
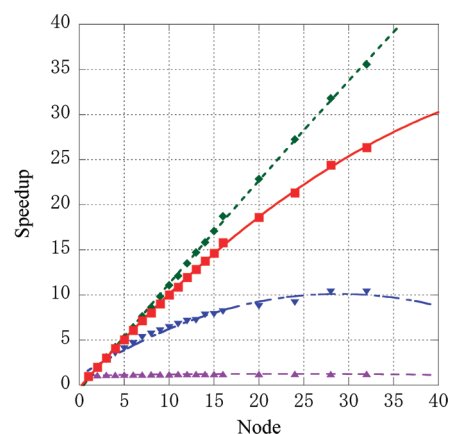

Figure 1. Speedup of the $[PtCl_4]^{2-}$ calculations. Inverted triangles (▼): 1-virtual part; diamonds (♦): 2-virtual part; triangles (▲): internal part; and squares (■): total.

increase in the number of nodes. The calculation for 1-virtual terms showed intermediate behavior: the speedup increased more slowly as the number of nodes increased. Table 2 also includes parallel efficiency, which is defined by $E(n) = S(n)/n$. The parallel efficiency was high for 2−32 nodes, as implied by the near proportionality of the speedup. The values were greater than 0.80.

The behaviors seen in the calculation of 1- and 2-virtual terms can be explained mainly by the fraction of computational time for the coupling coefficients $\langle A|E_X|B^M \rangle$ occupying by the computation

Table 3. d−d Excitation Energies of $[PtBr_4]^{2-}$ (eV)

state	ref-CI	GMC-QDPT	ref (%)[a]	TDDFT	band	expt
$1A_{1g}$	1.94	1.75	76.9	1.93		
$1A_{2g}$	1.99	1.81	76.9	1.97	1	2.11
$1E_g$	2.00	1.85	76.9	2.01	1	2.11
$1B_{2g}$	2.04	2.01	77.4	2.11		
$1B_{1g}$	2.32	2.13	77.0	2.19		
$2E_g$	2.36	2.23	77.0	2.29	2	2.37
$2A_{1g}$	2.98	2.50	76.0	2.66	3	2.81
$3E_g$	2.98	2.60	76.5	2.67	3	2.81
$2A_{2g}$	3.29	2.83	76.4	2.82	4	3.02
$2B_{1g}$	3.23	2.99	76.0	2.72		
$4E_g$	3.52	3.15	76.4	3.06	5	3.32
$2B_{2g}$	3.57	3.37	76.2			

[a] The reference weight of the ground state was 78.2%.

Table 4. d−d Excitation Energies of $[PtCl_6]^{2-}$ Calculations (eV)

state	ref-CI	GMC-QDPT	ref (%)[a]	TDDFT	expt
$1E_g$	3.49	2.25	64.8	2.43	
$1T_{2g}$	3.57	2.31	64.8	2.50	2.23
$1T_{1g}$	3.62	2.36	65.0	2.49	
$1A_{2g}$	4.16	2.68	65.0	2.63	
$2T_{1g}$	4.17	2.76	65.0	2.72	2.64
$2E_g$	4.42	2.93	64.5	2.74	
$2T_{2g}$	4.56	3.04	64.4	2.73	
$3T_{1g}$	4.53	3.05	64.7	2.79	
$2A_{2g}$	4.66	3.12	64.2	2.88	
$3T_{2g}$	5.05	3.47	64.5	2.87	3.51

[a] The reference weight of the ground state was 68.5%.

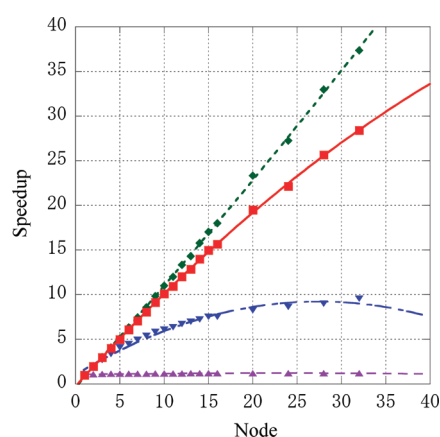**Figure 2.** Speedup of the $[PtBr_4]^{2-}$ calculations. Inverted triangles (▼): 1-virtual part; diamonds (◆): 2-virtual part; triangles (▲): internal part; and squares (■): total.

of each term. In the parallel algorithm explained in Section 2.2, the computational time required for the coupling coefficients was presumed to be small, and thus the coefficients are computed in each node. The speedup can be roughly estimated according to eq 8. For the 2-virtual term, this presumption was satisfactory. The computational time for CCs was only 0.31 s and hence $S(n)$ was close to n. By contrast, for the 1-virtual part, the presumption was not satisfactory. The computational time for CCs was 7.65 s, which was 5.6% of the time required for the 1-virtual term on one node (137.01 s) but 58% on 32 nodes (13.21 s). The computational times of CCs were therefore not negligible in multiple-node calculations, and as a result the $S(n)$ curve behaved as seen in Figure 1.

3.2. d−d Excitation Energies of Platinum Tetrabromide Dianion $[PtBr_4]^{2-}$. The second example was $[PtBr_4]^{2-}$. The computational details were similar to those for $[PtCl_4]^{2-}$. The target excited states of $[PtBr_4]^{2-}$ were the 12 excited states resulting from d−d single excitations. The reference space was of MRS type constructed from 20 electrons and 28 spinors comprising mostly d spinors of the platinum atom. The determinants that spanned the reference space were prepared in the same manner as in the $[PtCl_4]^{2-}$ calculation. The lowest 180 spinors were frozen in the perturbation calculations.

The computed excitation energies are summarized in Table 3 together with the experimental data of Kroening and co-workers[29]

and the TDDFT results.[28] For the states for which experimental data are available ($2A_{1g}$, $1A_{2g}$−$2A_{2g}$, and $2E_g$−$4E_g$ states), the computed values were in good agreement with the experimental values, as in the case of $[PtCl_4]^{2-}$. The maximum and average deviations from the experiment were 0.26 and 0.19 eV, respectively. The GMC-QDPT calculated values were close to the TDDFT values of Wang and Ziegler. Both results were somewhat small compared with the experimental values.

Figure 2 is a plot of speedup ratios. The speedup and parallel efficiency for $[PtBr_4]^{2-}$ showed similar trends to those found in $[PtCl_4]^{2-}$. The parallel efficiency was greater than 0.85 for n in the range 2−32.

3.3. d−d Excitation Energies of Platinum Hexachloride Dianion $[PtCl_6]^{2-}$. The third example was $[PtCl_6]^{2-}$, which is a d^6 octahedral complex. The target states were the lowest 10 excited states resulting from d−d single excitations as well as the ground state. The reference space was of MRS type constructed from 16 electrons and 24 spinors mostly comprising d spinors of the platinum atom. The determinants that spanned the reference space were generated from 65 parent configurations (the DHF configuration and the singly excited configurations constructed from the highest 16 occupied and the lowest 4 unoccupied spinors) and then selected according to their weights in the reference functions. The lowest 128 spinors were frozen in the perturbation calculations.

The computed results are summarized in Table 4 together with the experimental[30,31] data and the TDDFT results.[32] State assignment in GMC-QDPT was done in O_h point group symmetry, and calculations were done in D_{4h} group symmetry. For this system, a few experimental numbers (2.23, 2.64, and 3.51 eV) were available, and these were computed to be 2.31, 2.76, and 3.47 eV by GMC-QDPT. Compared with the $[PtCl_4]^{2-}$ and $[PtBr_4]^{2-}$ cases, the reference weights were slightly lower because the present calculation involved more correlated electrons. For the same reason, the differences between the reference CI and GMC-QDPT excitation energies were larger: The average difference was 0.18 eV in the $[PtCl_4]^{2-}$ case compared with 1.43 eV in the $[PtCl_6]^{2-}$ case.

Figure 3 is a plot of speedup for $[PtCl_6]^{2-}$ calculations. Unlike the previous cases, speedup of the 1-virtual term was almost proportional to the number of nodes. The total computational time for $[PtCl_6]^{2-}$ calculation was 7584.54 s and about five times larger than the former two systems. Therefore, the computational time for the CCs (11.90 s) was negligible. As a result, the total speedup and parallel efficiency for larger n was better than
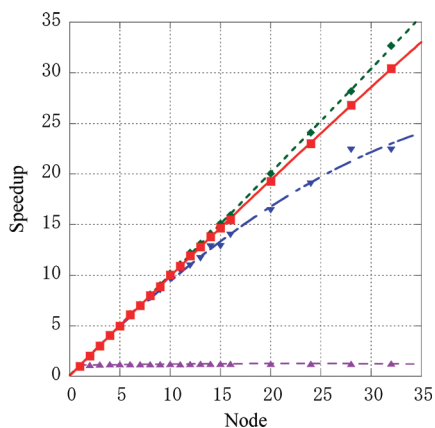
Figure 3. Speedup of the $[PtCl_6]^{2-}$ calculations. Inverted triangles (▼): 1-virtual part; diamonds (♦): 2-virtual part; triangles (▲): internal part; and squares (■): total.

Figure 4. Speedup of the Rn atom calculations. Inverted triangles (▼): 1-virtual part; diamonds (♦): 2-virtual part; triangles (▲): internal part; and squares (■): total.

Table 5. p−s and p−p Excitation Energies of the Rn Atom (eV)

configuration	term	ΔJ	ref-CI	GMC-QDPT	ref (%)[a]	SAOP	ΔSCF (LDA)	expt
$6p^5(^2P^o_{3/2})7s$	$^2[3/2]^o$	2	7.08	6.73	82.9	6.54	6.56	6.77
		1	7.26	6.93	83.4	6.74	6.72	6.94
$6p^5(^2P^o_{3/2})7p$	$^2[1/2]$	1	8.30	8.22	83.4			8.21
		0	8.71	8.79	85.8			8.64
$6p^5(^2P^o_{3/2})7p$	$^2[5/2]$	2	8.37	8.30	83.6			8.26
		3	8.53	8.50	84.0			8.43
$6p^5(^2P^o_{3/2})7p$	$^2[3/2]$	1	8.58	8.55	83.9			8.46
		2	8.63	8.63	84.4			8.52
$6p^5(^2P^o_{1/2})7s$	$^2[1/2]^o$	0	11.24	10.51	77.1	10.03	10.74	10.66
		1	11.29	10.52	79.2	10.11	10.61	10.79
$6p^5(^2P^o_{1/2})7p$	$^2[1/2]$	1	12.56	11.98	81.7			
		0	12.65	12.09	80.1			
$6p^5(^2P^o_{1/2})7p$	$^2[3/2]$	1	12.75	12.21	80.1			
		2	12.75	12.24	82.1			

[a] The reference weight of the ground state was 87.2%.

the previous cases. The parallel efficiency for $n = 32$ in the present case was 0.95, which was better than in the $[PtCl_4]^{2-}$ (0.82) and $[PtBr_4]^{2-}$ (0.89) cases.

3.4. 6p−7p and 6p−7s Excitation Energies of the Radon Atom. The last example is the excitation energies of the radon atom. The target states were the 14 excited states resulting from 6p−7s and 6p−7p single excitations as well as the ground state. The reference space was of multireference singles and doubles (MRSD) type constructed from six electrons and 14 spinors (corresponding to 6p, 7s, and 7p orbitals). The determinants that spanned the reference CI space were generated from the DHF $(6p)^6(7s)^0(7p)^0$ configuration and selected according to their weights in the reference functions. All spinors were included in the perturbation calculation.

The computed results are summarized in Table 5 together with experimental values[33] and TDDFT [statistical average of the orbital model exchange−correlation potential (SAOP) and ΔSCF] results[34] for the 6p−7s excitations. For the lowest four 6p−7s excitations, experimental values of 6.77 eV ($\Delta J = 2$), 6.94 eV

($\Delta J = 1$), 10.66 eV ($\Delta J = 0$), and 10.79 eV ($\Delta J = 1$) are available. These excitation energies were computed to be 6.73, 6.93, 10.51, and 10.52 eV, respectively. The former two values were in very good agreement with the experimental values, whereas the latter two had larger errors. For the latter two states, the reference weights were relatively low, and the excitation energies at the reference space CI level were too large, which indicates that the reference functions were of low quality compared with those of the other excited states. This was because the main characteristics of these states were not well expressed using the MRSD-type reference space generated from the DHF configuration. The present results had better accuracy than the TDDFT results. The TDDFT with SAOP underestimated 6p−7s excitation energies by 0.68 eV at most, compared with the experimental values. In addition, the computed values for the six lowest 6p−7p excited states were also in good agreement with experimental data, and the maximum deviation was 0.15 eV.

Figure 4 is a plot of speedup ratios for the internal, 1-virtual, and 2-virtual terms. Speedup of the calculation for 2-virtual terms, which is the bottleneck of the calculation, was nearly proportional to the number of nodes. The parallel efficiency value for $n = 32$ was 0.81, which was somewhat worse than those for the $[PtBr_4]^{2-}$ and $[PtCl_6]^{2-}$ cases. The wall time for the 1-virtual terms (355.38 s) was close to that for the 2-virtual terms (469.09 s), and it was not proportional to the number of nodes, as in the previous cases. Consequently, the speedup and parallel efficiency values were a little worse than the previous cases.

4. CONCLUSION

We have developed a new, efficient parallel algorithm for four-component relativistic GMC-QDPT introducing Kramers symmetry. Our new algorithm has two advantages. The first advantage is speeding up the calculation, which is expected to be linear with the number of computational nodes n. The second is a reduction in the memory resources required to $1/n$ compared with single-node calculations. In addition, because of the Kramers restriction, the amount of memory required to store two-electron integrals, which are necessary for perturbation calculations, was reduced to three-eighths of the requirement for conventional GMC-QDPT calculations.

We applied our new scheme to calculation of the d−d excitation energies of the platinum halide complexes, $[PtCl_4]^{2-}$,

1004

dx.doi.org/10.1021/ct2000205 |*J. Chem. Theory Comput.* 2011, 7, 998–1005

$[PtBr_4]^{2-}$, and $[PtCl_6]^{2-}$ and 6p−7s and 6p−7p excitation energies of the Rn atom. The present parallel algorithm had high efficiency, approximately proportional to the number of nodes. In GMC-QDPT calculations, the main bottleneck is calculation of the 2-virtual terms. Our new algorithm works linearly for these terms. Overall, the present algorithm showed high performance. In the case of platinum halide complexes, the calculated results were in good agreement with experimental values. We analyzed the wave function to evaluate our selection of reference functions. The reference weights were large enough for each state, and their deviations were small. Thus, these calculations have a good quality and balance. For the Rn atom, computational values of the two lower states of the 4 calculated 6p−7s excited states showed good agreement with the experimental values, while the computational values of 2 higher states had larger errors, and the reference weights were slightly smaller than for the lower two states.

■ AUTHOR INFORMATION

Corresponding Author

*E-mail: nakano@ccl.scc.kyushu-u.ac.jp.

■ REFERENCES

(1) Johnson, W. R.; Idrees, M.; Sapirstein *J. Phys. Rev. A* **1987**, *35*, 3218–3226.

(2) Ishikawa, Y. *Phys. Rev. A* **1990**, *42*, 1142–1150.

(3) Quiney, H. M.; Grant, I. P.; Wilson, S. *J. Phys. B* **1990**, *23*, L271.

(4) Blundell, S. A.; Johnson, W. R.; Sapirstein *J. Phys. Rev. Lett.* **1991**, *65*, 1411–1414.

(5) Dyall, K. G. *Chem. Phys. Lett.* **1994**, *224*, 186–194.

(6) Visscher, L.; Saue, T.; Nieuwpoort, W. C.; Fægri, K., Jr.; Gropen, O. *J. Chem. Phys.* **1993**, *99*, 6704–6715.

(7) Watanabe, Y.; Matsuoka, O. *J. Chem. Phys.* **2002**, *116*, 9585–9590.

(8) Eliav, E.; Kaldor, U. *J. Phys. Rev. A* **1994**, *49*, 1724–1729.

(9) Visscher, L.; Dyall, K. G.; Lee, T. J. *Int. J. Quantum Chem., Symp.* **1995**, *29*, 411–419.

(10) Fleig, T.; Jensen, H. J.; Olsen, J.; Visscher, L. *J. Chem. Phys.* **2006**, *124*, 104106.

(11) Fleig, T.; Olsen, J.; Marian, C. M. *J. Chem. Phys.* **2001**, *114* 4775–4790.

(12) Fleig, T.; Olsen, J.; Visscher, L. *J. Chem. Phys.* **2003**, *119* 2963–2971.

(13) Fleig, T.; Sorensen, L. K.; Olsen, J. *Theor. Chem. Acc.* **2007**, *118*, 347–356.

(14) Nakano, H.; Uchiyama, R.; Hirao, K. *J. Comput. Chem.* **2002**, *23*, 1166–1175.

(15) Miyajima, M.; Watanabe, Y.; Nakano, H. *J. Chem. Phys.* **2006**, *124*, 044101.

(16) Ebisuzaki, R.; Watanabe, Y.; Nakano, H. *Chem. Phys. Lett.* **2007**, *442*, 164–169.

(17) Umeda, H.; Koseki, S.; Nagashima, U.; Schmidt, M. W. *J. Comput. Chem.* **2001**, *22*, 1243–1251.

(18) Yanai, T.; Harrison, R. J.; Nakajima, T.; Ishikawa, Y.; Hirao, K. *Int. J. Quantum Chem.* **2007**, *107*, 1382–1389.

(19) Yanai, T.; Nakajima, T.; Ishikawa, Y.; Hirao, K. *J. Chem. Phys.* **2001**, *114*, 6526–6538; **2002**, *116*, 10122–10128.

(20) Abe, M.; Iikura, H.; Kamiya, M.; Nakajima, T.; Yanagisawa, S.; Yanai, T. *REL4D*; University of Tokyo: Tokyo, 2004.

(21) Yanai, T.; Kamiya, M.; Kawashima, Y. et al. *UTCHEM*; University of Tokyo: Tokyo, 2004.

(22) Koga, T.; Tatewaki, H.; Matsuoka, O. *J. Chem. Phys.* **2001**, *115*, 3561–3565. Koga, T.; Tatewaki, H.; Matsuoka, O. *J. Chem. Phys.* **2002**, *117*, 7813–7814.

(23) Dyall, K. G. *Theor. Chem. Acc.* **2002**, *108*, 335–340. Dyall, K. G. *Theor. Chem. Acc.* **2006**, *115*, 441–447.

(24) Sterzel, M.; Autschbach, J. *Inorg. Chem.* **2006**, *45*, 3316–3324.

(25) Kroening, R. F.; Rush, R. M.; Martin, D. S., Jr.; Clardy, J. C. *Inorg. Chem.* **1974**, *13*, 1366–1373.

(26) Granovsky, A. *Firefly*, version 7.1.G; Firefly Software: Austin, TX, 2009; http://classic.chem.msu.su/gran/firefly/index.html.

(27) Patterson, H. H.; Godfrey, J. J.; Khan, S. M. *Inorg. Chem.* **1972**, *11*, 2872–2878.

(28) Wang, F.; Ziegler, T. *J. Chem. Phys.* **2005**, *123*, 194102.

(29) Kroening, R.; Rush, R. M.; Martin, D. S., Jr.; Clardy, J. C. *Inorg. Chem.* **1974**, *13*, 1366–1373.

(30) Yoo, R. K.; Keiderling, T. A. *J. Phys. Chem.* **1990**, *94*, 8048–8055.

(31) Jørgensen, C. K. *Acta Chem. Scand.* **1956**, *10*, 518–534.

(32) Wang, F.; Ziegler, T. *J. Chem. Phys.* **2005**, *123*, 154102.

(33) Moore, C. E. *Atomic Energy Levels, National Bureau of Standards Circular 467*; U.S. Government Printing Office: Washington, D.C., 1949, 1952, 1958.

(34) Gao, J.; Liu, W.; Song, B.; Liu, C. *J. Chem. Phys.* **2004**, *121* 6658–6666.